A Review of Current Differences in Medical Imaging: Focus on MRI, CT, and DR

Zisheng Wang *

Jiangsu Tianyi High School, Wuxi, China

* Corresponding Author Email: peterwzs@hotmail.com

Abstract. Magnetic resonance imaging (MRI), computed tomography (CT), and digital radiogra- phy (DR) are primary medical imaging technologies that act as core diagnostic tools needed in modern practices. But the public's grasp of these technologies is often muddled, leading to several misunderstandings about their mechanism of action, uses and safety profiles. These modalities differ significantly in data acquisition and imaging principles, we will discuss the non-irradiant approach of MRI versus the radiation-based methods of CT and DR, we simulate the relaxation dynamics and imaging parameters to understand the uniqueness of each of the techniques, from superb soft tissue contrast of MRI, well-defined visualization of high-density structures in CT, and practical utility of a DR for fast diagnostics. In addition to healthcare described above, the potential use of X-ray and neutral particle beams for security screening and industrial imaging applications is also described, to give a wider view of the current status and future directions for these technologies.

Keywords: MRI, CT, DR, Medical Imaging, Radiation Safety.

1. Introduction

Today, Magnetic Resonance Imaging (MRI), Computed Tomography (CT), and Digital Radiography (DR) are the cornerstones of medical imaging technologies. The first two modalities have complementary strengths with different clinical applications. CT is better for visualizing bone fractures, tumors, and diseases that impact high-density soft tissue structures; MRI is unsurpassed when imaging structures such as muscles, ligaments, and brain tissue. DR remains the first-line imaging test for most diagnostic examinations, such as chest imaging. These tools are widely used in hospitals and imaging centers worldwide and have significantly enhanced diagnostic accuracy.

Despite their widespread use, public understanding of these technologies is often limited, leading to misconceptions about their safety and applications. This gap in understanding is further complicated by the overlapping applications of these imaging modalities and the nuanced ways they are presented to the public. The widespread use of these technologies has led to misunderstandings about their overlapping applications and how they are presented to the public.

A common misconception about MRI is that its original name Nuclear Magnetic Resonance Imaging (NMRI) was changed to MRI in English- speaking countries because the word" nuclear" is not commonly associated with a safe diagnostic technique. In Chinese, MRI is commonly referred to as 'ci gong zhen cheng xiang' (Magnetic Resonance Imaging), avoiding the term 'nuclear,' which has contributed to public concerns about radiation safety.

While CT and DR use ionizing radiation, MRI relies on magnetic fields and radio waves, making it a safer option in terms of radiation exposure. As a result, the radiation problem produces anxiety among patients regarding CT and DR safety quotients [1] [2].

In addition to radiation exposure, the differences between these imaging modalities in terms of their imaging duration, and diagnostic specificity are frequently not clear to patients and occasionally to health providers. The lack of exposure to these diagnostic tests leads to their underutilization making them underappreciated despite their utility in the management of the diagnosis and treatment of diseases [3].

This paper addresses some of these issues by explaining how MRI, CT, and DR images are formed based on key principles of imaging, specifically taking a closer look at the quantum me- chanical underpinnings of the MRI process. We simulate relaxation phenomena and perform a comparative

analysis of the imaging parameters to emphasize the differences of each modal- ity. Moreover, we discuss prospective applications outside the clinical arena such as industrial quality control, security screening, and material analysis, thereby illustrating the wider societal impact of these imaging technologies.

2. Methodology

2.1. Section Headings

Magnetic Resonance Imaging (MRI) uses the physical law of nuclear magnetic resonance (NMR), which is mainly used for detecting hydrogen protons in the human body [4]. This elementary quantum mechanical process consists of a few important, high-level steps:

Spin and Magnetic Moment: The hydrogen nuclei(protons) have an intrinsic angular mo-mentum, or spin, which corresponds to a magnetic moment (μ) . This relation is given by:

$$\mu = \gamma J \tag{1}$$

Where γ is the gyromagnetic ratio (42.58 MHz/T for hydrogen) and J is the spin angular momentum.

Magnetic Field Interaction: Given a strong external B_0 magnetic field (1.5T or 3T, usu- ally), those protons either align parallel (lower energy state) or anti-parallel (higher energy state) to the field lines. This is written as the energy difference between them:

$$\Delta E = \hbar \gamma B 0 \tag{2}$$

Where \hbar is the reduced Planck constant.

Proton Distribution: Boltzmann's Distribution describes the number of protons in either energy state. Since the protons can be in one of the two energy states, the number of protons at each state is given by Boltzmann's Distribution. For this, we define the ratio of $N\uparrow$ (the total number of protons in the higher energy state) to $N\downarrow$ (total number of protons in the lower energy state) by:

$$\frac{N_{\uparrow}}{N_{\rm l}} = e^{-\Delta E/k_{\rm B}T} \tag{3}$$

Where kB is the Boltzmann constant and T is the absolute temperature.

At body temperature (310 K) and for a field strength of 1.5 T, this leads to a small population difference of around 1 in 100,000 protons, but given the huge number of protons in biological tissue (about 1026 protons per cubic centimeter) this results in a detectable net magnetization (M₀) given by:

$$M_0 = \frac{N\gamma^2\hbar^2 B_0}{4kBT} \tag{4}$$

Where N is the total number of protons per unit volume.

The net magnetization is the foundation of an MRI signal, with the magnitude directly proportional to the external magnetic field B_0 .

Precession: The protons experience precession about the primary magnetic field direction at the Larmor frequency(ω_0) given by:

$$\omega \theta = \gamma B \theta \tag{5}$$

Radiofrequency Excitation: An RF (radiofrequency) pulse at Larmor frequency is trans- mitted towards the protons that in resonance with the Larmor frequency, release energy ener- gizing the protons and rotating the net magnetization to transverse plane. The absorbed energy can be expressed by this formula:

$$E = \hbar f = \hbar \omega 0 = \hbar \gamma B 0 \tag{6}$$

Where \hbar is Planck's constant and f is the frequency.

Here, the absorbed energy is equal to the energy difference between protons in two states, which corresponds to prediction in quantum mechanics.

Relaxation Processes: After suppression of the radiofrequency (RF) pulse, two simultaneous relaxation processes occur with different physical mechanisms and imaging consequences:

T1 Relaxation (Longitudinal): T1 relaxation is the phenomena in which excited protons lose energy to their surrounding molecular lattice (spin-lattice interaction) restoring longitudinal magnetization. Heat is transferred from the spinning protons to the environment, especially neighboring molecules that have rotational and vibrational frequencies comparable to the protons. T1 recovery (as per molecular mobility and local magnetic field fluctuation) occurs in an exponential formula:

$$Mz(t) = M0(1 - e - t/T1)$$
 (7)

T1 values that are characteristic of specific tissues based on their molecular composition and mobility. Oxygen being incorporated in fat molecules has an efficient energy transfer mechanism by operating at Larmor frequencies (rotatedacional states of its carbon-hydrogen bonds) leading to short T1 values (rapid recovery). On the other hand, free water with high molecular mobility has inefficient energy exchange, which results in longer T1 values. In T1-weighted images, this physical difference becomes visible, so that Tissues with short T1 are bright (fat), while Tissues with long T1 are dark (cerebrospinal fluid) [5].

T2 Relaxation (Transverse): Transverse spin decay occurs over a Timescale due to dephasing. In contrast to T1, which describes energy exchange, T2 relaxation describes predominantly loss of entropy due to spin-spin interactions. When this occurrence is fulfilled, the protons will be in phase after the RF pulse, generating coherent transverse magnetization. But variations in local magnetic fields due to nearby protons and molecular interactions disturb that coherence. Protons start to precess at slightly different frequencies, leading to progressive phase dispersion that behaves according to an exponential decay:

$$Mxy(t) = M0e - t/T2 \tag{8}$$

The dephasing reflects fundamental properties of the tissue microenvironment. Tissues with higher local field heterogeneities (for example, white matter with arranged myelin) lead to a faster dephasing (i.e. shorter T2) due to susceptibility effects. In contrast, homogeneous environments (e.g., pure water) let protons preserve coherence longer, leading to longer T2 times. In T2-weighted images, long T2 tissues (neuronal fluid) are bright, while short T2 tissues (white matter) are dark [5].

These unique physical mechanisms permit the normal pathological tissue distinction in clinical applications. Pathologic processes that result in increased water content or the loss of orderly tissue architecture (eg, inflammation, edema, tumors) usually prolong both T1 and T2 times, creating prototypical signal patterns that allow exact diagnosis and tissue characterization in MR imaging.

2.2. CT Imaging Principles

CT (Computed Tomography) uses X-rays to create cross-sectional images of body parts. CT uses ionizing radiation in its imaging, but clinically it should be used with ALARA (As Low as Reasonably Achievable) principle. Vulnerable populations such as pediatrics and pregnant females are more sensitive to radiation and should be evaluated for images having clinical justification with alternate imaging modalities. CT imaging relies on the attenuation of X-rays and produces two-dimensional grayscale images using the Beer-Lambert law; however, it does not permit the visualization of all tissue types. Based Principle It is dependent on the Beer-Lambert law:

$$I = I_0 e^{-\mu x} \tag{9}$$

Where I_0 is the X-ray intensity before the tissue, I am the intensity after traversing the tissue, μ is the linear attenuation coefficient, and x is the thickness of the tissue.

The X-ray tube rotates around the patient and acquires a series of projections, that are then reconstructed into cross-sectional images based on filtered back-projection or iterative reconstruction

algorithms. The resulting three-dimensional image reflects tissue density within Hounsfield Units (HU)—wherein water is 0 HU and air -1000 HU.

Traditionally, filtered back projection (FBP) is used for CT image reconstruction which is less computationally intensive but results in noise in images at low radiation doses. While modern CT systems utilize iterative reconstruction algorithms that compare and adjust the reconstructed image until it becomes satisfactory, such objectives were not possible to achieve with film systems. This algorithm improves an initial guess of the image (often the FBP image) iteratively comparing the X-ray projections simulated from the current guess with the measured image projections. This process is repeated until image noise and motion artifact are reduced, with preservation of anatomical detail.

There are several distinct advantages of these algorithms in clinical practice. First, they substantially attenuate quantum noise by introducing statistical models of photon detection to allow for dose reductions in the range of 30–60%, without disturbing image quality for diagnostic purposes. Secondly, they efficiently diminish streak artifacts from high-density materials (such as metal implants), and beam hardening effects that can greatly corrupt FBP images. Finally, advanced implementations utilize sophisticated physical models such as the detector response functions, scatter correction, and beam spectrum characteristics to achieve better spatial resolution and low-contrast detectability. Commercial offerings range from statistical iterative reconstruction (where noise modeling can be emphasized) to model-based iterative reconstruction (where all components of optics and physics that describe the system are incorporated) [6].

The applications, such as pediatric imaging, screening examinations, and repeat follow-up studies, benefit the most clinically. Iterative techniques have been shown to preserve diagnostic confidence at ultra-low-dose protocols (sub-millisievert chest CT) that would yield prohibitively noisy images with conventional FBP. But such advantages do not come without trade-offs. Aside from their higher computational demands, iterative reconstructions also create images with a different noise texture, which is sometimes referred to by radiologists as "plastic" or "artificial," potentially masking subtle pathologies [7]. Moreover, the level of noise reduction (strength setting) needs to be analytically adapted to the individual anatomical region and clinical application. The main trade-off is still computation complexity, but this limitation has been largely mitigated by modern hardware in clinical settings.

2.3. DR Imaging Principles

Digital Radiography (DR) is the latest advance in conventional X-ray imaging. It uses X- rays like CT, but it only takes a single projection instead of multiple cross-sections. Similar to CT, X-rays are differentially attenuated depending on tissue density and atomic number as they pass through the body (Beer-Lambert relationship).

Instead of photographic film, DR uses digital detectors to detect the transmitted X-rays (indirect or direct conversion systems) [8].

Two-step X-ray detection process is used for indirect conversion systems [9]. First, the X-ray photons are absorbed by a scintillator material (commonly cesium iodide (CsI) or gadolinium oxysulfide (GOS)), converting the X-ray energy to visible light. Then, an array of photodiodes registers this light, converting the optical signals to electrical charges. These charges are digitized into the final image. The columnar geometry of CsI can counteract some of the lateral spread of the light, allowing for a more sophisticated spatially-resolved readout, which would be lost, at least in part, in the light piping to a photo-detector, although due to the multiple conversion stages some signal loss is unavoidable.

In contrast, direct conversion systems utilize one-step processing; X-ray photons directly convert into electrical charges created in a photoconductor layer (typically a photoconductor such as amorphous selenium (a-Se)). X-rays interacting with the photoconductor create electron-hole pairs collected by an applied electric field. Theoretically, this mechanism provides better spatial resolution, as it omits the light diffusion effects present in indirect systems.

It converts it into digital electronic signals while film- based imaging uses photographic film for this purpose. This data is subsequently transformed into a digitized two-dimensional image that has advantages in dynamic range, post-processing and lower radiation dose than film-based radiography [10].

3. Results and Analysis

3.1. Comparative Analysis of Imaging Parameters

Our analysis reveals significant differences in key imaging parameters among MRI, CT, and DR technologies, as summarized in Table 1.

Parameter	MRI	CT	DR
Radiation Type	Non-ionizing (RF waves)	Ionizing (X-rays)	Ionizing (X-rays)
Radiation Dose	None	2-10 mSv (typical)	0.1-1 mSv (typical)
Imaging Time	15-60 minutes	5-30 seconds	0.1-1 second
Primary Contrast	Proton density	Electron density	Tissue density
Mechanism T1/T2 relaxation		(atomic number)	atomic number
Cost Factor (relative) High		Moderate	Low

Table 1. Comparison of Key Imaging Parameters

Note: Radiation dose values are sourced from "Radiation Dose in X-Ray and CT Exams" (RadiologyInfo.org, 2023, American College of Radiology)

MRI differs in its use of non-ionizing radiation, which avoids radiation exposure, but in-volves much longer imaging times. CT enables fast imaging with superior bony detail but at higher radiation doses. DR is the fastest and least expensive of X-ray modalities, and visits to the radiology unit contribute an acceptable dose of radiation to the patient when used for routine diagnostic indications.

3.2. Simulation of MRI Relaxation Dynamics

In order to illustrate the physics of MRI contrast mechanisms, we modeled T1 recovery and T2 decay for three representative tissue types: gray matter, white matter, and cerebrospinal fluid (CSF), all of which fall within different ranges of values for tissue T1, T2, and proton density. The simulation references known, established relaxation time constants at 1.5T field strength (Table 2).

The simulation accurately modeled the recovery of T1 and decay of T2 curves using the exact equations that describe the underlying physics of the MRI:

$$Mz(t) = MO(1 - e - t/T1)$$
 (10)

$$Mxy(t) = M0e - t/T2 \tag{11}$$

Table 2. Tissue Relaxation Times at 1.5T

Tissue	T1 (ms)	T2 (ms)
Gray Matter	1124 ± 50	95 ± 8
White Matter	884 ± 50	72 ± 4
Blood	1441 + 120	95 + 8

Data source: [11] Stanisz GJ, Odrobina EE, Pun J, Escaravage M, Graham SJ, Bronskill MJ, Henkelman RM. T1, T2 relaxation and magnetization transfer in tissue at 3T. Magnetic Resonance in Medicine, 2005; 54 (3): 507 - 512.

Python code was developed based on these equations to describe precise time-dependent relaxation curves for each tissue. The simulation time ranged from 0 to 3000ms incrementing by 5ms each step, which allowed the relaxation behavior of each tissue to be fully accounted for.

```
Code: import numpy as np
import matplotlib.pyplot as plt
def addNoise (data, amplitude=0.02):
   noise = np.random.normal (0, amplitude, data.shape)
   return data + noise
def plotAngledRange (plotObj, center, deviation, level, color):
   lower = center - deviation
   upper = center + deviation
   angle = np.pi/6
   y_offset = 0.02
   plotObj.plo t ([lower, center], [level-y offset, level], color=color, linewidth=2)
   plotObj.plot ([center, upper], [level, level-y_offset], color=color, linewidth=2)
   cap_length = 0.01
   plotObj.vlines(x=[lower, upper], ymin=level-y_offset-cap_length,
               ymax=level-y_offset+cap_length, color=color, linewidth=2)
timepoints = np.linspace (0, 3000, 1000)
brainRegions = {
    'White Matter': {
       'T1': (884, 50), 'T2': (72, 4),
       'color': '#0077BE',
       'labelpos': (-80, 20),
       'T2labelpos': (-20, -20)
     },
     'Gray Matter': {
         'T1': (976, 67), 'T2': (95, 8),
         'color': '#4D4D4D',
         'labelpos': (10, -20),
         'T2labelpos': (20, 20)
     },
     'Blood': {
         'T1': (1441, 120), 'T2': (95, 8),
         'color': '#CC0000',
         'labelpos': (10, 20),
         'T2labelpos': (20, -20)
     }
}
brainScan, (recoveryPlot, decayPlot) = plt.subplots (1, 2, figsize=(16, 7))
brainScan.patch.set_facecolor ('white')
for region, characteristics in brainRegions. items ():
  relaxationTime, deviation = characteristics ['T1']
```

```
Volume 149 (2025)
```

```
magnetization = addNoise (1 - np.exp(-timepoints/relaxationTime))
       recoveryPlot.plot (timepoints, magnetization, label=region, color=characteristics ['color'],
linewidth=3)
       marker63 = -relaxationTime * np.log (1 - 0.63)
       plotAngledRange (recoveryPlot, marker63, deviation, 0.63, characteristics['color'])
       recoveryPlot.annotate (f'{relaxationTime}±{deviation}ms',
                     xy=(marker63, 0.63),
                     xytext=characteristics['labelpos'],
                     textcoords='offset points',
                     bbox=dict (facecolor='white', edgecolor=characteristics['color'], alpha=0.9))
    recoveryPlot.axhline (y=0.63, color='k', linestyle='--', alpha=0.3)
    whiteRegion = brainRegions ['White Matter']
    decayTime, decayDev = whiteRegion ['T2']
    decaySignal = addNoise(np.exp(-timepoints/decayTime))
    decayPlot.plot (timepoints, decaySignal, label='White Matter', color=whiteRegion['color'],
linewidth=3)
    marker37 = -decayTime * np.log (0.37)
    plotAngledRange (decayPlot, marker37, decayDev, 0.37, whiteRegion ['color'])
    decayPlot.annotate (f'{decayTime}±{decayDev}ms',
                   xy=(marker37, 0.37),
                   xytext=whiteRegion ['T2labelpos'],
                   textcoords='offset points',
                   bbox=dict (facecolor='white', edgecolor=whiteRegion['color'], alpha=0.9))
    mixedTissueColor = '#8B4513'
    combinedDecayTime = 95
    combinedDecayDev = 8
    combinedSignal = addNoise (np.exp (-timepoints/combinedDecayTime))
    decayPlot.plot
                      (timepoints,
                                      combinedSignal,
                                                          label='Gray
                                                                                    &
                                                                                         Blood'.
                                                                         Matter
color=mixedTissueColor, linewidth=3)
    mixedMarker = -combinedDecayTime * np.log (0.37)
    plotAngledRange (decayPlot, mixedMarker, combinedDecayDev, 0.37, mixedTissueColor)
    decayPlot.annotate (f'{combinedDecayTime})±{combinedDecayDev}ms',
                   xy = (mixedMarker, 0.37),
                   xytext=(20, 20),
                   textcoords='offset points',
                   bbox=dict(facecolor='white', edgecolor=mixedTissueColor, alpha=0.9))
    decayPlot.axhline (y=0.37, color='k', linestyle='--', alpha=0.3)
    for plot in [recoveryPlot, decayPlot]:
       plot.set_xlabel ('Time (ms)', fontsize=10)
```

```
plot.set_ylabel ('Signal Intensity (a.u.)', fontsize=10)
plot.grid (True, linestyle='--', alpha=0.3)
plot.spines ['top'].set_visible (False)
plot.spines ['right'].set_visible (False)
plot.legend (loc='upper left', frameon=True, fancybox=True, shadow=True)

recoveryPlot.set_title ('T1 Recovery Analysis', pad=12, fontsize=12)
decayPlot.set_title ('T2 Decay Analysis', pad=12, fontsize=12)

plt.suptitle ('Advanced Brain Tissue Relaxation Analysis at 1.5T', fontsize=12, y=0.92)

plt.tight_layout ()
plt.subplots_adjust (top=0.85)
plt.show ()
```

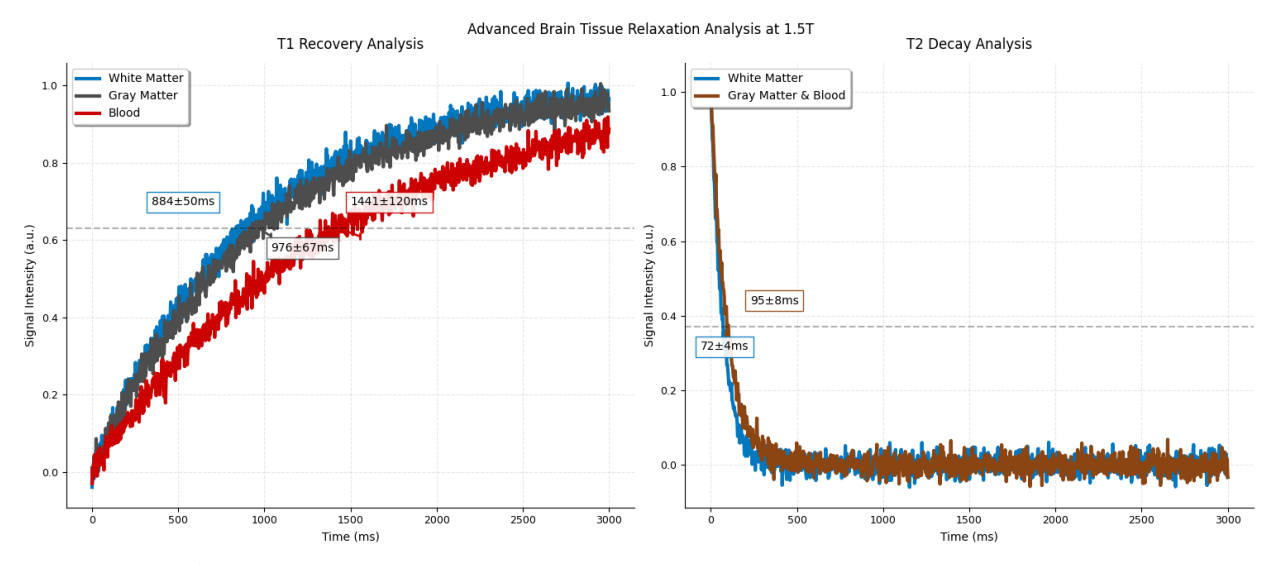


Figure 1. Simulated T1 Recovery and T2 Decay curves for brain tissues.

Simulated Brain Tissues and Blood T1 Recovery and T2 Decay Curves and Calculated Relaxation Times at 1.5 T—Left panel: T1 recovery curves for the various tissues calculated from T1 relaxation times (white matter, 884±50ms > gray matter, 976±67ms > blood, 1441±120ms) indicate that tissues with shorterT1times recover faster than those with longert1values. Right; T2 decay curves of tissues, where tissues with longer T2 times (gray matter and blood (95±8ms)) maintain signal longer than white matter (72±4ms). The 63% recovery line for T1 and 37% decay line for T2 represent the time points at which magnetization reaches 63% of its maximum value for T1 recovery and 37% of its initial value for T2 decay, respectively. They highlight the defining time constants of each tissue, with error bars representing measurement uncertainties.

The simulation illustrates the effect on the various tissues and why they all give rise to various signal intensities in T1 and T2-weighted PET images. In T1 of white matter, shows the brightest appearance because white matter has shorter T1 time (884±50ms) than blood (1441±120ms), so blood appears darker. For T2-weighted imaging, gray matter and blood are bright with long T2 times (95±8ms), while white matter is dark with a shorter T2 time (72±4ms). The error bars in the plots reflect the experimental uncertainties in these measurements, which illustrate the natural variability of tissue properties.

These results from simulation models explain the excellent soft tissue contrast capability available through MRI imaging modalities especially for neuroimaging applications where small differences

in the same concentration of tissue must be imaged directly. The ability to manipulate pulse sequences to enhance T1 or T2 contrast allows flexibility not possible with CT or DR.

3.3. Clinical Application Analysis

Our analysis of clinical applications revealed distinct strengths for each imaging modality, as summarized in Table 3.

Clinical Need	Preferred Modality	Rationale
Brain Tumor Detection	MRI	Superior soft tissue contrast, multiplanar capabilities
Acute Stroke	CT (initial), MRI (follow-up)	CT: rapid accessibility for hemorrhage detection; MRI: superior for early infarct detection
Bone Fractures	CT or DR	Excellent bone detail, rapid acquisition [12] [13]
Lung Imaging	DR (initial), CT (detailed)	DR: quick overview; CT: detailed evaluation of nodules [14]
Spinal Disc Herniation	MRI	Excellent visualization of disc material and neural compression [15]
Cardiac Imaging	MRI or CT	MRI: functional assessment without radiation; CT: coronary artery evaluation

Table 3. Primary Clinical Applications

This distribution of applications demonstrates how each technology fills specific clinical niches based on its intrinsic strengths and limitations.

4. Conclusion

MRI is a non-ionizing modality that leverages the principles of nuclear magnetic resonance, distinctively differentiating it from CT and digital radiography, as explained in the present study, that further has highlighted core divergences in action across these diagnostic imaging modali- ties. The imaging parameters comparison and MRI relaxation dynamics simulation work together, giving insight into how and why these modalities are superior in certain clinical situations.

Different imaging modalities have different physical properties and practical considerations which allow them to fill different clinical niches. The multiparametric imaging capabilities of MRI afford functional assessment and tissue characterization in addition to the primary goal of anatomical visualization, information that is particularly valuable in both oncology and neurology where microstructural changes precede gross pathology. However, CT's volumetric acquisition and multiplanar reformation capabilities have now broadened the uses of CT to include complex surgical planning and quantitative analysis of disease progression. Plus, DR's portability and broad availability, especially in remote settings and for bedside examinations requiring immediate clinical decision, guarantees its long-term relevance. This ideal deployment of complementary technologies along a clinical pathway maximizes both the diagnostic yield and efficient use of resource within 21st-century healthcare systems.

These technologies have enormous potential, not just in healthcare. As such, MRI methods are of interest for non-destructive testing in an industrial quality control context, where there are no concerns over radiation exposure. CT has been most commonly used in security screening at airports, and industrial metrology for accurate dimensional measurements. DR still works in veterinary medicine, forensic analysis and art authentication.

In the future, MRI scanning will go faster based on using parallel imaging and compressed sensing; CT will work at a lower radiation dose by employing iterative reconstruction al- gorithms; while DR technology will improve image quality by incorporating advanced post- processing techniques. The widespread adoption of artificial intelligence across all modalities will enhance both diagnostic accuracy and workflow efficiency.

Together, the different physical principles of MRI, CT, and DR give them distinct capabil- ities, and that; understanding their bases can inform their optimal use in clinical care and their potential use in other fields. These knowledge does not only uncloud the public misconceptions around these technologies, but also guides their future development and implementation as to maximize the potential benefits to society.

References

- [1] Brenner DJ, Hall EJ. Computed Tomography An Increasing Source of Radiation Exposure. New England Journal of Medicine, 2007; 357 (22): 2277 2284.
- [2] Smith-Bindman R, Lipson J, Marcus R, et al. Radiation Dose Associated with Common Computed Tomography Examinations and the Associated Lifetime Attributable Risk of Cancer. Archives of Internal Medicine, 2009; 169 (22): 2078 2086.
- [3] Schauer DA, Linton OW. NCRP Report No. 160, Ionizing Radiation Exposure of the Population of the United States. Medical Physics, 2009; 36 (11): 5305 5309.
- [4] Bushberg JT, Seibert JA, Leidholdt EM, Boone JM. The Essential Physics of Medical Imaging. 3rd Edition. Lippincott Williams & Wilkins, 2011.
- [5] McRobbie DW, Moore EA, Graves MJ, Prince MR. MRI from Picture to Proton. 3rd Edition. Cambridge University Press, 2017.
- [6] Kalender WA. Computed Tomography: Fundamentals, System Technology, Image Quality, Applications. Publicis Publishing, 2011.
- [7] Boas FE, Fleischmann D. CT Artifacts: Causes and Reduction Techniques. Imaging in Medicine, 2012; 4 (2): 229 240.
- [8] Hendee WR, Ritenour ER. Medical Imaging Physics. 4th Edition. Wiley-Liss, 2002.
- [9] Seibert JA, Boone JM. X-ray Imaging Physics for Radiologic Technologists. Radiologic Technology, 2005; 76 (5): 417 439.
- [10] Krupinski EA. Digital Radiography Image Quality: Image Processing and Display. Journal of the American College of Radiology, 2007; 4 (6): 390 400.
- [11] Stanisz GJ, Odrobina EE, Pun J, Escaravage M, Graham SJ, Bronskill MJ, Henkelman RM. T1, T2 relaxation and magnetization transfer in tissue at 3T. Magnetic Resonance in Medicine, 2005; 54 (3): 507 512.
- [12] Padhani AR, Liu G, Koh DM, Chenevert TL, Thoeny HC, Takahara T, Dzik-Jurasz A. Diffusion-Weighted Magnetic Resonance Imaging as a Cancer Biomarker: Consensus and Recommendations. Neoplasia, 2009; 11 (2): 102 125.
- [13] Goo HW, Goo JM. Dual-Energy CT: New Horizon in Medical Imaging. Korean Journal of Radiology, 2017; 18 (4): 555 569.
- [14] Dobbins JT, McAdams HP. Chest Radiography: Digital and Conventional. Radiology, 2003; 227 (1): 11 25.
- [15] Kuhl CK, Traber F, Schild HH. Whole-Body High-Field-Strength (3.0-T) MR Imaging in Clinical Practice. Part I. Technical Considerations and Clinical Applications. Radiology, 2008; 246 (3): 675 696.